Modeling of Conjunctive Two-Dimensional Surface-Three-Dimensional Subsurface Flows

Masaru Morita[1] and Ben Chie Yen, F.ASCE[2]

Abstract: In the rainfall-runoff process, interaction between surface and subsurface flow components plays an important role, especially in rainwater abstraction and overland flow initiation at the early stage of rainfall events. Coupling of surface and subsurface flow submodels, therefore, is necessary for advanced comprehensive and sophisticated rainfall-runoff simulation. This article presents a conjunctive two-dimensional (2D) surface and three-dimensional (3D) subsurface flow model, which uses the noninertia approximation of the Saint-Venant equations for 2D unsteady surface flow and a modified version of the Richards equation for 3D unsteady unsaturated and saturated subsurface flows. The equations are written in the form of 2D and 3D heat diffusion equations, respectively, and solved numerically. The surface and subsurface flow components are coupled interactively using the common boundary condition of infiltration through the ground surface. The conjunctive model is verified with Smith and Woolhiser's experimental data (reported in 1971) of initially dry and initially wet soil. Subsequently the model is applied to a hypothetical soil plot of clay or sand to simulate the overland flow, infiltration, and subsurface flow for four different rainfalls. The conjunctive model contributes as a tool for improved detailed simulation of 2D surface and 3D subsurface flows and their interaction.

DOI: 10.1061/(ASCE)0733-9429(2002)128:2(184)

CE Database keywords: Surface flow; Subsurface flow; Three-dimensional flow; Two-dimensional flow; Models; Rainfall.

Introduction

Many watershed runoff models have been developed to simulate unsteady surface flows. In most of these surface runoff models, however, interaction between surface and subsurface flows is ignored and the subsurface flow contribution is approximated by using an infiltration formula such as that of Horton (1933) or Philip (1957). Conversely, in subsurface flow modeling of infiltration and porous medium flow, the effect of nonuniform pressure head from spatially varying surface flow is usually not directly and explicitly considered. This separated modeling approach to the surface and subsurface components of watershed runoff is acceptable for catchments where the permeability of the subsurface soil is relatively low and the time scales for the surface and subsurface flows are significantly different (Freeze 1972a; Yen and Riggins 1991). Otherwise, interaction between the two flow components plays an important role, especially on the initial loss of rainfall and on overland flow initiation. Wallach et al. (1997) used a one-dimensional (1D) surface and three-dimensional (3D) subsurface flow model to investigate the error in surface flow from ignoring interaction between the two flow components and found that neglecting the interaction overestimates surface flow depth during the rising part of the hydrograph and underestimates it during the recession part. Therefore, coupling the surface and subsurface flow components is necessary for improved comprehensive and sophisticated watershed modeling.

Horton (1933; 1935) was one of the earliest to describe the role of infiltration in the rainfall-runoff process. Rubin and Steinhardt (1963) were among the first to study infiltration and ponding prior to overland flow initiation. They described the relation among rainfall, infiltration, and ponding as a problem of setting the boundary condition for the partial differential equation of unsaturated subsurface flow. They suggested that an incessant rainfall results in ponding only if rainfall intensity exceeds the saturated soil's hydraulic conductivity. However, they neither dealt numerically with the case of ponding nor showed how to solve the equation for the commencement of ponding and runoff. Hanks and Bower (1962) were among the earliest to show that computer-based numerical techniques can be a useful tool to study the process of infiltration into heterogeneous soils. Reviews of the principles governing the infiltration process can be found in Philip (1969) and Swartzendruber and Hillel (1973). Reeder et al. (1980) showed the effect of varying surface water depth on infiltration by examining one-dimensional downward infiltration and percolation in unsaturated homogeneous soil. Smith and Woolhiser (1971) indicated, by coupling of surface and subsurface flow components, that overland flow occurs when the top soil layer becomes saturated. This concept of overland flow initiation has been widely adopted by conjunctive modelers. Smith and Woolhiser (1971) also made mention of resetting the upper boundary condition if available surface water plus rainfall is less than potential infiltration when the surface water depth is receding. Their study, however, gave no specific description on ''potential infiltration.'' Yen and Akan (1984) adopted the concept of ''infiltrability'' (infiltration capacity), and described overland flow initiation based on rainfall intensity exceeding infiltrability.

[1]Professor, Dept. of Civil Engineering, Shibaura Institute of Technology, Shibaura, Minato-ku, Tokyo 108-8548, Japan. E-mail: morita@sic.shibaura-it.ac.jp

[2]Professor, Dept. of Civil and Environmental Engineering, Univ. of Illinois at Urbana-Champaign, Urbana, IL 61801.

Note. Discussion open until July 1, 2002. Separate discussions must be submitted for individual papers. To extend the closing date by one month, a written request must be filed with the ASCE Managing Editor. The manuscript for this paper was submitted for review and possible publication on July 14, 2000; approved on June 19, 2001. This paper is part of the ***Journal of Hydraulic Engineering***, Vol. 128, No. 2, February 1, 2002. ©ASCE, ISSN 0733-9429/2002/2-184–200/$8.00+$.50 per page.

Classification of Conjunctive Surface and Subsurface Flow Modeling

Conjunctive modeling of surface and subsurface flows can be classified according to the number of spatial dimensions considered for the two flow components. With the advent of digital computers, several models have been developed to simulate the overland surface flow together with the subsurface flow. As shown in Table 1, most of them consider one-dimensional (1D) surface flow with 1D or 2D subsurface flow. Freeze (1972a) simulated 1D open channel flow with 3D subsurface flow. A well known watershed-scale model SHE (Abbott et al. 1982 and 1986; Bathurst 1995), as well as an Italian model by Di Giammarco et al. (1994) allows 2D surface flow and 1D vertical unsaturated above 2D horizontal saturated subsurface flows. Whereas its later version MIKE SHE (Refsgaard and Storm 1995) allows 1D unsaturated and 3D saturated subsurface flows; however, the internal boundary condition between the surface and top soil ''root zone'' remains assumed instead of being part of the solution. Bradford and Katopodes (1998) simulated 2D subsurface flow together with 2D overland flow in vertical and longitudinal directions. Natural watersheds generally have heterogeneous surface and soil conditions for which surface runoff can be simulated as depth averaged 2D flow while the subsurface flows should be simulated three dimensionally. Reliable simulation will be very useful in solving today's various types of problems concerning water quantity and quality of storm runoff. It can be seen from Table 1 that no conjunctive model has been reported to simulate two-dimensional surface and three-dimensional unsaturated and saturated subsurface flows simultaneously and iteratively, considering the internal boundary condition interactively as part of the solution.

The alternative to grouping the models based on their spatial dimensions is to classify them by considering how the surface and subsurface components are coupled mathematically. The highest level is to numerically solve all the equations for the surface flow, subsurface flow, and the common internal boundary condition between the two in tandem as a set of simultaneous equations. This set of equations is solved at a time step before advancing to the next time step. This approach of true simultaneous total coupling is, however, a rather difficult and challenging problem still to be explored. No study on it has been reported in the literature.

The next level of coupling is to solve the surface flow equations and subsurface flow equations separately but iteratively at the same time step, interlinked by a gradient-type equation representing the exchange (infiltration) as the common internal boundary condition between the surface and subsurface flows. Solution for the surface and subsurface flows at a time step is achieved when the iteration errors fall within specified tolerances before the computation is advanced to the next time step. This approach of conjunctive modeling will be referred to as *alternating iterative coupling*. Five models of this type reported in the literature are summarized in Table 1(a).

The third, conjunctive modeling approach which is the simplest but also the least accurate is by solving the surface flow submodel and subsurface flow submodel separately in succession without iteration between the submodels [Table 1(b)]. Freeze (1972a) called this uncoupled conjunctive approach *externally coupled*. The surface flow model is usually solved first because of the relatively short runoff period and rapid change of flow. The result is passed on to solve the subsurface flow at the same time step before advancing to solve the surface flow at the next time step. The discretization time scale used for the subsurface flow often is much larger than that for the surface flow (Freeze 1972a; Liggett and Dillon 1985; Yen and Riggins 1991; Wallach et al. 1997).

A further simplification of the externally coupled approach is to express the vertically downward 1D subsurface flow as an algebraic infiltration equation such as the Horton, Philip or Green-Ampt formulas, instead of a partial differential equation for the unsaturated soil, i.e., without solving the subsurface flow equations. This simplified, no coupling approach is popular in border-irrigation studies; some of the published models are summarized in Table 1(c).

Many water resources problems, such as agricultural runoff and pollutant transport, watershed surface runoff generation, urban infiltration through porous pavement and trenches, hill slope stability under rainfall, irrigation flow, and groundwater recharge from rainfall often involve three-dimensional surface and subsurface flows. To simulate such flows, a conjunctive depth-averaged 2D surface and 3D subsurface model is required. This paper describes the hydraulic aspects of a conjunctive 2D surface-3D subsurface flow model using a theoretical treatment of the infiltrability as the interface between the two flow components. Analysis of various numerical schemes and the alternating iteractive coupling used for the model can be found in a companion paper (Morita and Yen 2000). To illustrate the use of the conjunctive model, simulations for two types of overland flow often considered by hydrologists, geomorphologists, and groundwater scientists, namely the infiltration-excess generated Hortonian overland flow and saturation generated overland flow, are presented to illustrate the interaction between surface and subsurface flows.

Governing Equations

In the current study, an approximated form of the dynamic wave equation, often known as the diffusion wave model (Akan and Yen 1981b)—henceforth referred to as the ''noninertia model'' (Yen and Tsai 2001)—is utilized to represent the two-dimensional surface flow, together with a modified version of the Richards equation is used for the three-dimensional variably saturated subsurface flow. The equations representing both flows are mathematically classified as a type of heat diffusion equation.

Surface Flow

The depth-averaged two-dimensional continuity equation for the surface flow is

$$\frac{\partial h}{\partial t}+\frac{\partial}{\partial x}(uh)+\frac{\partial}{\partial y}(vh)+i-r=0 \tag{1}$$

where h = flow depth; u and v = depth average velocity components in the x and y directions, respectively; i = infiltration rate; and r = rain intensity.

The momentum conservation relationship can be written as

$$\frac{\partial}{\partial t}(uh)+\frac{\partial}{\partial x}(u^2h)+\frac{\partial}{\partial y}(uvh)+ru_{rx}$$

$$+g\cdot h\cdot\frac{\partial h}{\partial x}-g\cdot h\cdot(S_{0x}-S_{fx})=0 \tag{2}$$

J. Hydraul. Eng. 2002.128:184-200.

Table 1. Selected Conjunctive Surface-Subsurface Flow Model

Investigator	Surface flow			Subsurface flow			Interface common boundary
	Dimension	Equation[a]	Solution Technique	Dimension	Equation	Solution Technique	
(a) Alternating interactive coupling models							
Pinder and Sauer (1971)	1D Rectangular channel	DW	Staggered explicit scheme	2D Horizontal	Saturated flow Eq.	ADI	Gradient-type infiltration Eq.
Freeze (1972a)	1D Rectangular channel	DW	Single step Lax–Wendroff	3D	Richards unsaturated & saturated	SLOR	Infiltration rate stream flow depth
Akan and Yen (1981a)	1D Overland	DW	4-point implicit	2D	Richards unsaturated & saturated	SLOR	Gradient-type infiltration rate quasiimplicit iteration
Schmitz et al. (1985)	1D Overland	DW	Implicit method of characteristics	1D	Quasianalytic Parlange	Algebraic FEM	Infiltration rate
Bradford and Katopodes (1998)	2D	Point Reynolds Eqs. $k-\varepsilon$	Marker-and-cell, moving grid	2D $(x-z)$	Richards	Gelarkin FEM	Common pressure and infiltration rate surface flow front location as iteration error control
(b) Externally coupled models							
Smith and Woolhiser (1971)	1D Overland	KW	Lax–Wendroff	1D	Richards unsaturated	Crank–Nicholson	Infiltration rate
Liggett and Dillon (1985)	1D Channel	KW	Muskingum–Cunge	1D	Laplace unsaturated	BIEM	do.
SHE (Abbott et al. 1982; 1986; Bathurst et al. 1995)	2D Overland	NI	Abbott 6-point implicit for SHE,	Unsaturated: 1D vertical	Richards	Full implicit	Root zone water budget
MIKE SHE (Refsgaard and Storm 1995)	1D Channel		Modified Gauss–Seidel for MIKE SHE	Saturated: 2D SHE Horizontal 3D (MIKE SHE)	Richards Boussinesq	Implicit, SOR (Also, preconditioned conjugated gradient for MIKE SHE)	Between saturated and unsaturated soils, iterative water table through water budget in saturated
Di Giammarco et al. (1994)	2D Overland	NI	Finite element, Crank–Nicholson or integrated	Unsaturated: 1D Vertical	Richards	Finite element	Darcy's law
	1D Channel		Finite difference, conjugated gradient method	Saturated: 2D Horizontal	Richards	Nonlinear algebraic Eqs.	Unsaturated soil column
Wallach et al. (1997)	1D Overland	KW	Implicit Newton iteration	1D	Richards	Implicit	Gradient-type infiltration rate
(c) Border irrigation models							
Katopodes and Strelkoff (1977)	1D	DW	Method of characteristic	1D	Kostiakov	Algebraic Eq.	Infiltration rate
Akanbi and Katopodes (1988)	2D	DW	Dissipative finite element with deforming grid	1D	Kostiakov	do.	do.
USDA-WEPP (Savadi 1993)	1D	KW		1D	Green–Ampt	do.	do.
Playan et al. (1994)	2D	DW	Leapfrog	1D	Kostiakov	do.	do.
Singh and Bhallamudi (1996)	1D	DW	MacCormack	1D	Kostiakov or Parlange–Haverkamp	do.	do.

[a]DW=Dynamic wave, NI=Noninertia wave, KW=Kinematic wave.

J. Hydraul. Eng. 2002.128:184-200.

$$\frac{\partial}{\partial t}(vh)+\frac{\partial}{\partial x}(uvh)+\frac{\partial}{\partial y}(v^2h)+ru_{ry}$$

$$+g\cdot h\cdot\frac{\partial h}{\partial y}-g\cdot h\cdot(S_{0y}-S_{fy})=0 \tag{3}$$

where g = gravitational acceleration; S_{0x} and S_{0y} = bottom slopes in the x and y directions, respectively; S_{fx} and S_{fy} = friction slopes in the x and y directions, respectively; and u_r = the velocity of rainwater when joining the surface flow. The following assumptions are made in deriving these two equations (Yen 1973): (1) the pressure distribution is hydrostatic over the depth; (2) correction coefficients for velocity distribution over the depth are equal to unity; (3) spatial gradients of the internal stresses (except pressure) acting on the depth are negligible; (4) the x and y components of the flow velocity of the rainfall or infiltration are small relative to the overland flow velocity such that the contribution of the lateral flows (i and r) to the momentum equations can be ignored. These two equations are often referred to as the complete (but not exact) dynamic wave equations (Yen 1973).

Various approximations of the dynamic wave equation have been proposed by dropping terms in the momentum equation to simplify the numerical computations. The simplest is the kinematic wave approximation, which is obtained by ignoring the inertia and pressure terms. It is suitable for long overland or channels with sufficient slope, but it cannot account for the effect of downstream backwater. The quasi-steady dynamic wave option is obtained by dropping only the local acceleration term; however, it offers practically no computational advantage over the dynamic wave. A reasonable compromise is the noninertia wave approximation which is obtained by ignoring the local and convective acceleration terms. With the pressure terms retained, the noninertia wave model is able to account for the downstream backwater effect. Akan and Yen (1981b) and others have shown that in most free surface flow cases, where the accelerations are not high, ignoring the inertia terms in Eqs. (2) and (3) greatly simplifies the computational efforts without sacrificing accuracy. Therefore, in this study the noninertia approximation is used. The noninertia approximation of Eqs. (2) and (3), neglecting the momentum contribution from rainfall and infiltration, yields

$$\frac{\partial h}{\partial x}-S_{0x}+S_{fx}=0 \tag{4}$$

$$\frac{\partial h}{\partial y}-S_{0y}+S_{fy}=0 \tag{5}$$

A flow resistance formula is needed for the friction slopes. Overland flow may occur in the low range of flow Reynolds number, for which Manning's n is not constant (Yen 1991). Therefore, the Darcy–Weisbach formula is adopted, thus

$$(S_{fx},S_{fy})=\left(f_d\frac{u^2}{8gh},f_d\frac{v^2}{8gh}\right) \tag{6}$$

The friction resistance coefficient f_d is calculated based on the Reynolds number, which is defined as $\mathrm{R}=V_mh/\nu$, where V_m = mean velocity over the depth and ν = kinematic viscosity (Yen and Akan 1999). For laminar flow with $\mathrm{R}<500$ and under rain intensity r

$$f_d=\left[24+660\left(\frac{r}{\sqrt[3]{g\nu}}\right)^{0.4}\right]\Big/\,\mathrm{R} \tag{7}$$

The effect of infiltration on the resistance is assumed negligible.

For transitional flow with $500<\mathrm{R}<30\,000$

$$f_d=\frac{0.223}{\mathrm{R}^{0.25}} \tag{8}$$

For turbulent flow with $\mathrm{R}>30\,000$

$$f_d=\frac{1}{4}\left[-\log\left(\frac{k_s}{12R}+\frac{1.95}{\mathrm{R}^{0.9}}\right)\right]^{-2} \tag{9}$$

where k_s = equivalent sand grain roughness size and R = hydraulic radius of the flow.

The overland surface slopes in Eqs. (4) and (5) can be related to overland surface elevation s as

$$(S_{0x},S_{0y})=\left(-\frac{\partial s}{\partial x},-\frac{\partial s}{\partial y}\right) \tag{10}$$

Further, by using the water surface elevation $H_s=h+s$ instead of the flow depth h, the following equations are obtained from Eqs. (4) and (5):

$$(S_{fx},S_{fy})=\left(-\frac{\partial H_s}{\partial x},-\frac{\partial H_s}{\partial y}\right). \tag{11}$$

By comparing Eqs. (6) and (11), uh and vh in Eq. (1) can be expressed as follows:

$$(uh,vh)=\left(-D_x\frac{\partial H_s}{\partial x},-D_y\frac{\partial H_s}{\partial y}\right) \tag{12}$$

in which D_x and D_y are described by Eq. (13) with f_d which is dependent on the Reynolds number R,

$$(D_x,D_y)=\left(\sqrt{\frac{8gh^3}{f_d}}\left|\frac{\partial H_s}{\partial x}\right|^{-1/2},\quad\sqrt{\frac{8gh^3}{f_d}}\left|\frac{\partial H_s}{\partial y}\right|^{-1/2}\right) \tag{13}$$

From the continuity equation (1) and Eq. (12), the governing equation for surface flow can be represented as follows:

$$\frac{\partial H_s}{\partial t}=\frac{\partial}{\partial x}D_x\frac{\partial H_s}{\partial x}+\frac{\partial}{\partial y}D_y\frac{\partial H_s}{\partial y}+r-i \tag{14}$$

In Eq. (14), the diffusion coefficients D_x and D_y change with the flow depth and velocity. The falling rain drops are assumed to be so small and numerous that one may treat the rainfall as a continuous body of water entering the soil (Rubin and Steinhardt 1963).

Subsurface Flow

The equation for three-dimensional variably saturated subsurface flow is represented on the basis of the Richards equation (Freeze and Cherry 1979)

$$\frac{\partial H}{\partial t}=\frac{\partial}{\partial x}\alpha_x(\theta)\frac{\partial H}{\partial x}+\frac{\partial}{\partial y}\alpha_y(\theta)\frac{\partial H}{\partial y}+\frac{\partial}{\partial z}\alpha_z(\theta)\frac{\partial H}{\partial z} \tag{15}$$

$$\alpha_i(\theta)=K_{si}K_r/(\partial\theta/\partial P) \tag{16}$$

where H = piezometric head; K_{sx}, K_{sy}, and K_{sz} = saturated hydraulic conductivity in the x, y, and z directions, respectively; K_r = relative hydraulic conductivity; P = capillary pressure head; θ = volumetric moisture content; $\theta=nS$; n = soil porosity; and S = saturation degree. The piezometric head H is related to P by $H=P+z$. Eq. (15) involves the following assumptions (Freeze and Cherry 1979): (1) the flow is Darcian and isothermal; (2) the porous medium is rigid and isotropic; (3) the velocity heads, in-

J. Hydraul. Eng. 2002.128:184-200.

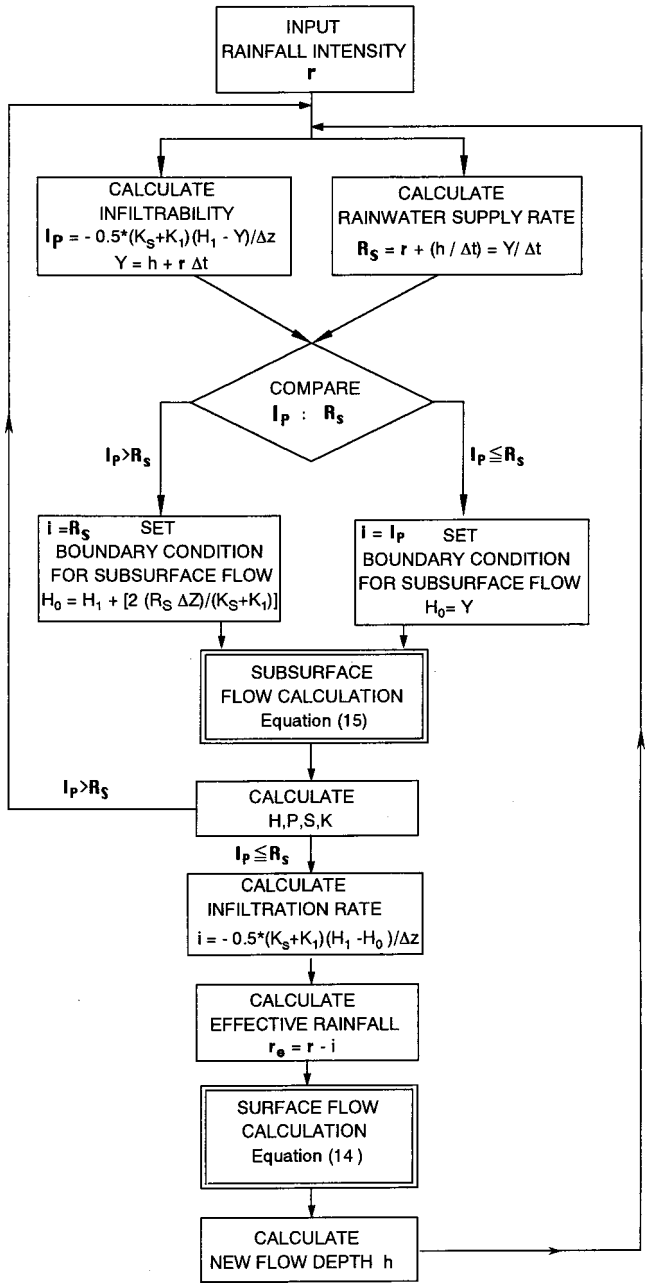

Fig. 1. Flow chart of surface-subsurface flow conjunctive model calculation

ternal forces, temperature gradients, osmotic gradients, and chemical concentration gradients are all negligible; and (4) the soil is nonhysteretic. In the analysis it is further assumed that the unsaturated soil is not swelling and the air phase is continuous and moves freely under atmospheric pressure.

Eq. (15) can be applied to both saturated groundwater flow and unsaturated soil water flow. For saturated flow, P is positive and K_r is unity. Except for the case of initial loss, the effect of surface flow on the subsurface flow can be treated by the surface boundary condition: flow depth. In calculation of unsaturated flow, a known relation among P, S, and K_r is required.

Infiltration as Common Internal Boundary Condition for Surface and Subsurface Flows

For coupling the 2D surface flow [Eq. (14)] interactively with the 3D subsurface flow [Eq. (15)], the infiltration between these two

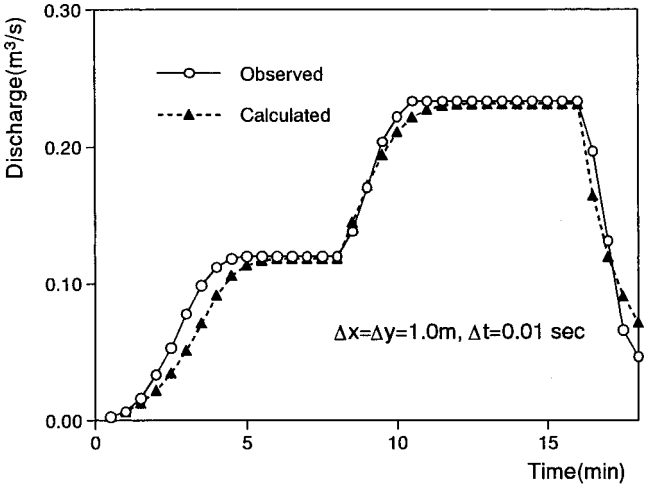

Fig. 2. Comparison of computed two-dimensional surface flow with Izzard's experimental discharge

phases is used as the common internal boundary condition to be solved iteratively. The infiltration is defined in a Darcian manner as

$$i = K_{sz} K_r \left.\frac{\partial H}{\partial z}\right|_{\text{ground surface}} \tag{17}$$

In an application, the infiltrability must be compared with the available water supply. The infiltrability is the potential infiltration rate or infiltration capacity under the condition of given surface water depth and soil water content just below the surface. For rain over an initially dry bed, surface flow does not start until the rainfall intensity r exceeds the infiltrability I_p, and Eq. (14) applies only after this condition, $r > I_p$. This checking procedure at each time step is shown in Fig. 1 and is described as follows:

1. Calculate the infiltrability I_p using Eq. (18)
$$I_p = -0.5(K_{sz} + K_1)(H_1 - Y)/\Delta z \tag{18}$$
where K_{sz} = saturated hydraulic conductivity; K_1 and H_1 = hydraulic conductivity and piezometric head at the first node in the z direction; and Δz = thickness of a thin layer of the top soil just below the soil surface in which the piezometric head varies approximately with depth. Pinder and Sauer (1971) called this the thickness of the bottom sediment; and Y = available water from rain and depth of flow at the surface calculated as a depth
$$Y = h + r\Delta t \tag{19}$$
where h = water depth at the previous time step; r = rain intensity; Δt = time increment. The water depth h is set to zero until ponding depth or overland flow occurs.
2. Calculate the water supply rate as
$$R_s = Y/\Delta t = r + (h/\Delta t) \tag{20}$$
3. Compare the infiltrability I_p with the water supply R_s.
4. If the infiltrability I_p is larger than the rainwater supply R_s, the actual infiltration rate is R_s and set the boundary condition at the surface for Eq. (15) as follows:
$$H_0 = H_1 + 2[R_s \Delta z/(K_{sz} + K_1)] \tag{21}$$
where H_0 = surface piezometric head at ground surface as the boundary condition.

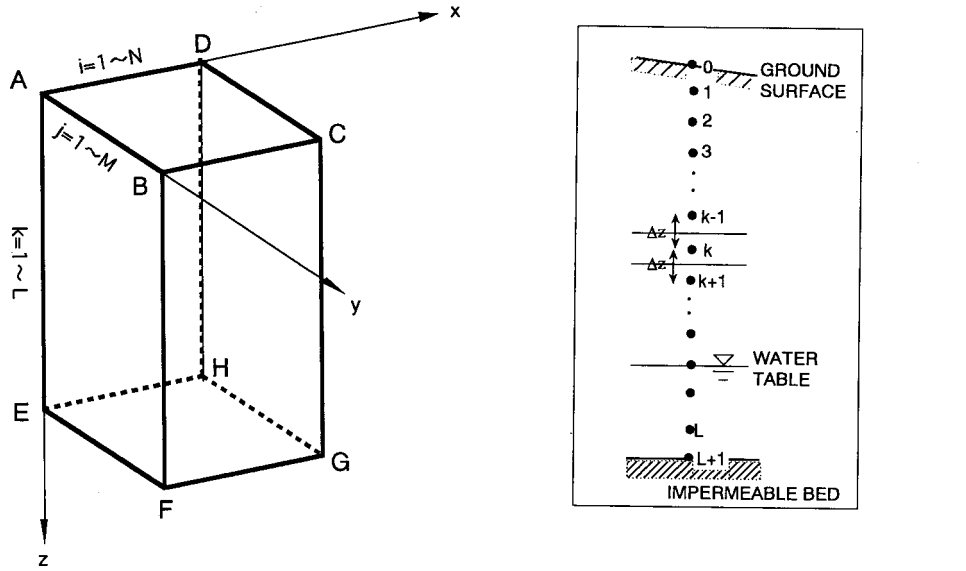

(a) Three-dimensional Computational Grid (b) Vertical Discretization in Subsurface Zone

Fig. 3. Computational grid for subsurface flow model

5. If the infiltrability I_p is less than the rainwater supply R_s, the actual infiltration rate is I_p and set the ground surface boundary condition for Eq. (15) as
$$H_0 = Y \tag{22}$$
6. Calculate the piezometric head H by Eq. (15) under the surface boundary condition from step 4 or step 5.
7. Go back to step 1 in the case of step 4. In the case of step 5, on the other hand, go to surface flow calculation by Eq. (14) with the infiltration rate $i = I_p$ to determine the new flow depth h and then go back to step 1.

Procedure 1–7 is repeated until the surface and subsurface flow solutions change within a specified acceptable tolerance before advancing to the next time step. Usually one cycle of iteration is sufficient, owing to the slow response of subsurface flow to the variation of surface flow depth.

The procedure shown in Fig. 1 is different from those of other existing models in coupling the two flow components, especially in dealing with overland flow initiation. In other conjunctive models, overland flow initiates when the top soil surface becomes saturated, while for this conjunctive model overland flow starts when the rain water supply exceeds the infiltrability. The former method is henceforth referred to as the ''saturation method,'' and the latter as the ''infiltrability method.'' The idea of comparison between rain intensity and infiltrability is well accepted for noncoupling models, such as those using the Horton infiltration equation. However, no previous conjunctive model is formulated in this manner. The present conjunctive model explicitly formulates the procedure and defines the infiltrability as a control parameter for the interaction between the two flow components.

Numerical Scheme for Conjunctive Surface-Subsurface Flow Model

The governing equations (14) and (15) for surface and subsurface flows, respectively, are written in the form of heat diffusion equations. Therefore, many numerical methods for solving two- and three-dimensional heat diffusion equations can be selected for this study. Based on an investigation of several numerical schemes reported in a companion paper (Morita and Yen 2000), a conjunctive model (Model 1 in that paper) with the Saul'yev (1964) downstream scheme for the 2D surface flow, Eq. (14), coupled with Larkin's (1964) alternating direction explicit (ADE) scheme for the 3D subsurface flow, Eq. (15), was selected for this paper. Those interested in the selected numerical schemes, as well as five other schemes for the surface submodel and four other schemes for the subsurface submodel, should refer to Morita and Yen (2000) for details.

By using Saul'yev's method, Eq. (14) for surface flow is written in finite difference form for a surface element (i,j) as follows:

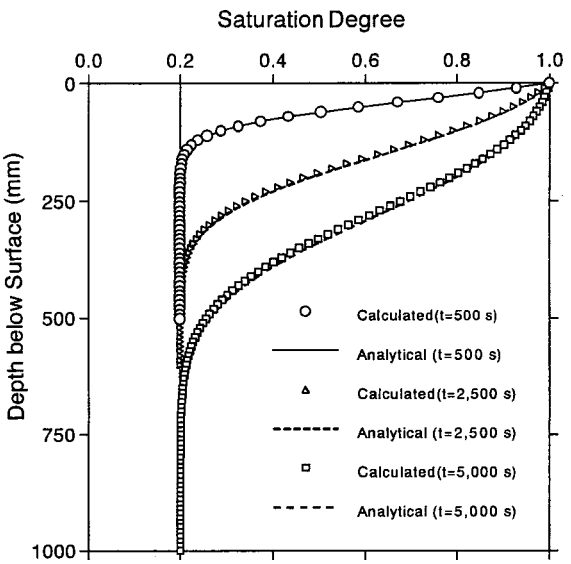

Fig. 4. Comparison between calculated soil saturation ($\Delta t = 1.0$ s) and Philip's analytical solution

J. Hydraul. Eng. 2002.128:184-200.

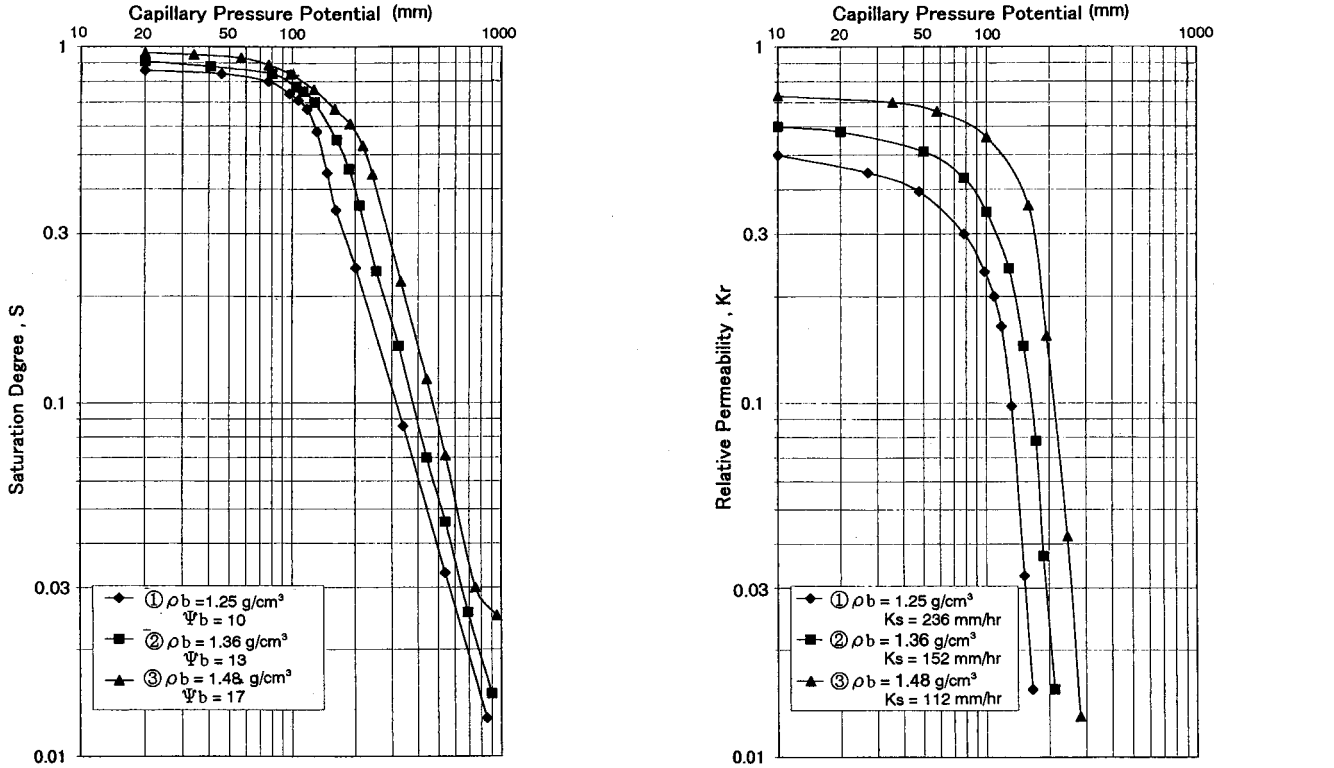

(a) Relation between Saturation Degree and Capillary Pressure

(b) Relation between Relative Permeability and Capillary Pressure

Fig. 5. Hydraulic properties of Smith and Woolhiser's (1971) unsaturated soils used in verification of conjunctive model

$$\frac{(H_S)_{i,j}^{t+\Delta t}-(H_S)_{i,j}^{t}}{\Delta t}=\frac{D_{x1}}{(\Delta x)^2}[(H_S)_{i-1,j}^{t+\Delta t}-(H_S)_{i,j}^{t+\Delta t}]+\frac{D_{x2}}{(\Delta x)^2}[(H_S)_{i+1,j}^{t}-(H_S)_{i,j}^{t}]+\frac{D_{y1}}{(\Delta y)^2}[(H_S)_{i,j-1}^{t+\Delta}-(H_S)_{i,j}^{t+\Delta t}]+\frac{D_{y2}}{(\Delta y)^2}[(H_S)_{i,j+1}^{t}-(H_S)_{i,j}^{t}] \quad (23)$$

In Eq. (23), D should be calculated as the average value of the two nodes, e.g., $D_{x1}=(D_{i-1,j}+D_{i,j})/2$.

Fig. 2 shows a typical comparison of numerically simulated result with the observed discharge hydrograph for Izzard's (1946) experiment Run 138. Izzard's experimental plot was 22 m (72 ft) long and 1.8 m (6 ft) wide, with a bed slope of 0.001. The surface was covered with crushed slate roofing paper. Surface runoff was produced by simulated uniform rainfall over the entire plot and discharge was measured at the downstream end of the plot. The surface flow in Izzard's experiment was practically one dimensional. Therefore, to verify the two-dimensional surface flow submodel in the present computation the plot was tilted at either 45 or 26.6° to the x direction in simulations. The simulated hydrograph in Fig. 2 is calculated by Saul'yev's method for the plot tilted at 45°.

For the subsurface flow, Eq. (15) is written in a finite difference form for an internal element (i,j,k) of the computational grid shown in Fig. 3 using Larkin's ADE method as

$$\frac{U_{i,j,k}^{t+\Delta t}-H_{i,j,k}^{t}}{\Delta t}=\frac{\alpha_{x1}}{(\Delta x)^2}(U_{i-1,j,k}^{t+\Delta t}-U_{i,j,k}^{t+\Delta t})+\frac{\alpha_{x2}}{(\Delta x)^2}(H_{i+1,j,k}^{t}-H_{i,j,k}^{t})+\frac{\alpha_{y1}}{(\Delta y)^2}(U_{i,j-1,k}^{t+\Delta t}-U_{i,j,k}^{t+\Delta t})+\frac{\alpha_{y2}}{(\Delta y)^2}(H'_{i,j+1,k}-H_{i,j,k}^{t})+\frac{\alpha_{z1}}{(\Delta z)^2}(U_{i,j,k-1}^{t+\Delta t}-U_{i,j,k}^{t+\Delta t})+\frac{\alpha_{z2}}{(\Delta z)^2}(H_{i,j,k+1}-H_{i,j,k}) \quad (24)$$

$$\frac{V_{i,j,k}^{t+\Delta t}-H_{i,j,k}^{t}}{\Delta t}=\frac{\alpha_{x1}}{(\Delta x)^2}(H_{i-1,j,k}^{t}-H_{i,j,k}^{t})+\frac{\alpha_{x2}}{(\Delta x)^2}(V_{i+1,j,k}^{t+\Delta t}-V_{i,j,k}^{t+\Delta t})+\frac{\alpha_{y1}}{(\Delta y)^2}(H_{i,j-1,k}^{t}-H_{i,j,k}^{t})+\frac{\alpha_{y2}}{(\Delta y)^2}(V_{i,j+1,k}^{t+\Delta t}-V_{i,j,k}^{t+\Delta t})+\frac{\alpha_{z1}}{(\Delta z)^2}(H_{i,j,k-1}^{t}-H_{i,j,k}^{t})+\frac{\alpha_{z2}}{(\Delta z)^2}(V_{i,j,k+1}^{t+\Delta t}-V_{i,j,k}^{t+\Delta t}) \quad (25)$$

$$H_{i,j,k}^{t+\Delta t}=\frac{U_{i,j,k}^{t+\Delta t}+V_{i,j,k}^{t+\Delta t}}{2} \quad (26)$$

Larkin's ADE method uses two intermediate values U and V to calculate H at the next time step. The moisture diffusivity α is calculated as the average value of the two nodes, e.g., α_{x1}

J. Hydraul. Eng. 2002.128:184-200.

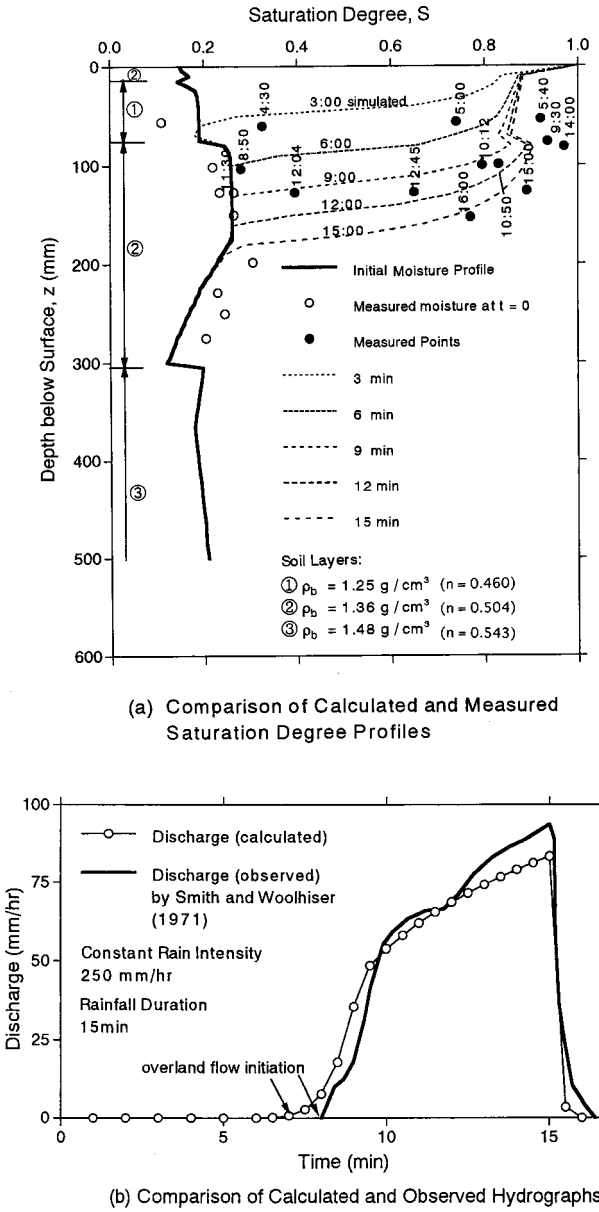

Fig. 6. Comparison of conjunctive-flow model simulated saturation degree and hydrograph with experimental data by Smith and Woolhiser (1971) for initially dry soil case

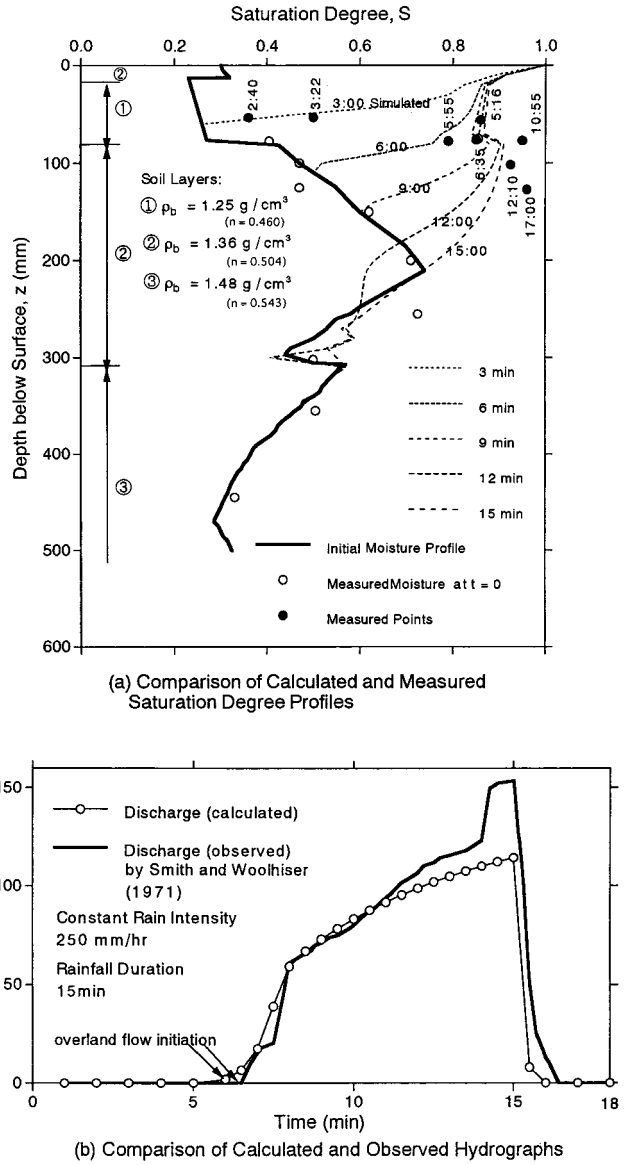

Fig. 7. Comparison of conjunctive-flow model simulated saturation degree and hydrograph with experimental data by Smith and Woolhiser (1971) for initially wet soil case

$=(\alpha_{i-1,j,k}+\alpha_{i,j,k})/2$. In these equations, the node numbers in the z direction, k, at the surface in Fig. 3 are zero if the surface has no slope. Otherwise, the numbers should be adjusted according to the topography of the surface. Fig. 4 shows an example comparison between numerically computed soil saturation profiles and Philip's analytical solution of 1D percolation. For details of soil conditions for this simulation, see Morita and Yen (2000).

Conjunctive Model Verification

The surface and subsurface flow submodels are coupled together with infiltration as the common internal boundary condition using the seven-step iterative coupling scheme previously described. Verifications of the surface and subsurface submodels were discussed in the companion article by Morita and Yen (2000). The only known published experimental data with sufficient details available for conjunctive model verification are those of Smith and Woolhiser (1971). In their experiment, a laboratory soil flume was used to observe surface runoff, infiltration, and soil moisture movement. The flume was 2 in. (51 mm) wide, 4 ft (1.22 m) deep and 40 ft (12.2 m) long. The simulated rainfall had a constant intensity of 9.9 in. (250 mm/h) over a duration of 15 min. The fluid used was light oil with viscosity close to that of water. In the simulation for verification, the kinematic viscosity was assumed to be 0.89×10^{-6} m^2/s and the flume slope was set at 0.01. The relationships between capillary pressure potential and saturation degree and relative hydraulic conductivity, respectively, of three different soils tested are depicted in Figs. 5(a and b). These soils were placed in three layers and tested with two different initial soil moisture profiles representing relatively dry and wet cases, respectively, as shown in Figs. 6(a) and 7(a). The soil moisture distribution was measured at a cross section 18.3 ft (5.58 m) from the upstream end and the discharge from the surface measured at

J. Hydraul. Eng. 2002.128:184-200.

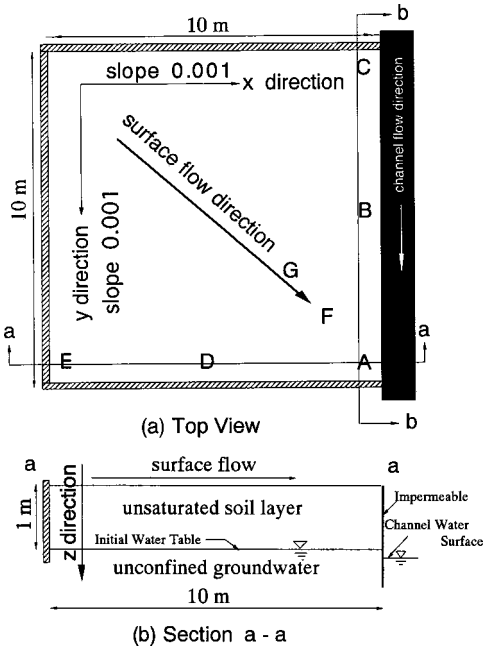

Fig. 8. Hypothetical drainage plot for conjunctive model simulation

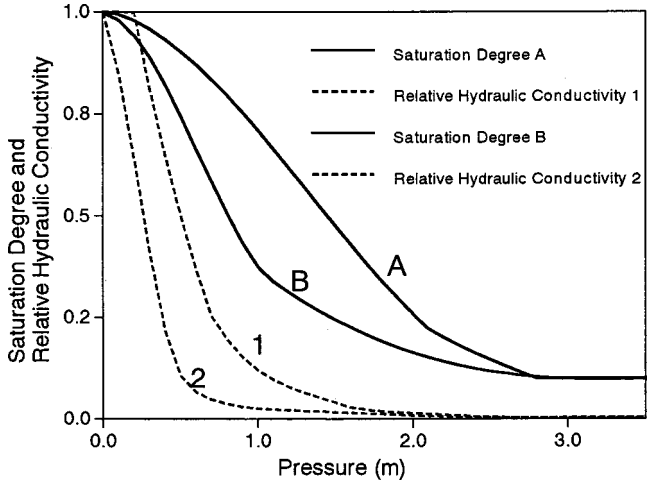

Fig. 9. Example of unsaturated soil hydraulic properties: clay type (A-1) and sand type (B-2)

the end of the flume. In the simulation the porosities of the soils for subsurface flow were assumed as given in Fig. 6.

For the dry case, the calculated moisture profiles and hydrograph from the conjunctive model are shown in Figs. 6(a and b) together with the experimental data. The computed soil saturation profiles shown in Fig. 6(a) depict the wetting front propagation of the vertical infiltration at three minute intervals. The calculated soil moisture curves match fairly well with the measured points except those with saturation degrees from 0.9 to 1.0. For the hydrograph in Fig. 6(b), the calculated result from the conjunctive model reproduces reasonably well the observed hydrograph although there is a discrepancy of about 1 min in overland flow initiation time between the two hydrographs.

For the wet case, Figs. 7(a and b) show the calculated and observed results of the moisture movement and hydrographs, respectively. Soil saturation profiles are given in the same way as in the dry case. Unfortunately, the wet case has fewer measured points for saturation degree less than 0.8 than for the dry case. The soil saturation profiles at 3:00 and 6:00 agree with the measured points. As in the dry case, the calculated curves have no agreement with the measured points with saturation degree from 0.9 to 1.0. The discrepancies may be explained partly because of insufficient information to describe the soil hydraulic properties at almost saturated conditions in Fig. 5. The rapid jump in the observed hydrograph in Fig. 7(b) near the end of the rainfall was likely caused by air compression (Smith and Woolhiser 1971). Apart from this discrepancy, the calculated hydrographs agree with the observed ones for both wet and dry cases, Figs. 6 and 7.

Without measured free surface flow profiles and soil moisture profiles at a number of soil depths at different times, the experimental data of Smith and Woolhiser were not designed for and are insufficient to verify simulation of the 2D nature of the surface runoff and the 3D characteristics of the subsurface flow by the conjunctive model. Nevertheless, previous testing reported in Morita and Yen (2000) revealed that in conjunctive modeling, the surface submodel dominates the numerical accuracy and stability, whereas the subsurface submodel dominates the computation time, suggesting the possibility and desirability of using a larger computational time increment for the subsurface submodel than the surface submodel, provided the soil hydraulic conductivity is not high.

Table 2. Input Data for Conjunctive Flow Model Simulations

Case	Soil data $K_s(10^{-3}$ mm/s) (Curve in Fig. 9)	Surface data Slope x	Slope y	Rainfall data Rain intensity (Hyetograph type)	Numerical grid data Δx (m) (N)	Δy (m) (M)	Δz (m) (L)	Result Figure
I	0.5 (Clay type)	0.001	0.001	100 mm/h (peak) (triangular)	1.0 (10)	1.0 (10)	0.01 (100)	Fig. 10(a) Fig. 12
II	0.5 (Clay type)	0.001	0.001	50 mm/h (constant) (rectangular)	1.0 (10)	1.0 (10)	0.01 (100)	Fig. 10(b) Fig. 11
III	5.0 (Sand type)	0.001	0.001	100 mm/h (peak) (triangular)	1.0 (10)	1.0 (10)	0.01 (100)	Fig. 13(a)
IV	5.0 (Sand type)	0.001	0.001	150 mm/h (peak) (triangular)	1.0 (10)	1.0 (10)	0.01 (100)	Fig. 13(b)
V	5.0 (Clay type)	0.05	0.04	150 mm/h (constant) (rectangular)	1.0 (10)	1.25 (8)	0.05 (50)	Fig. 14 –Fig. 17

J. Hydraul. Eng. 2002.128:184-200.

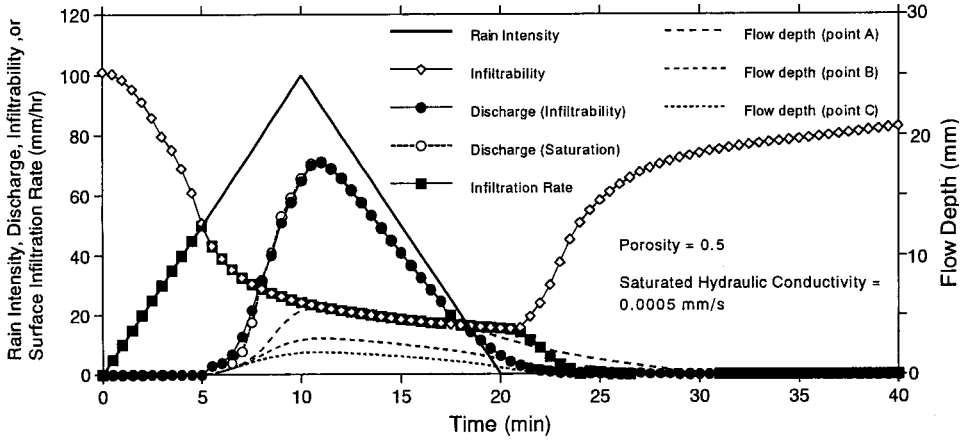

(a) Simulated Results from Triangular Hyetograph

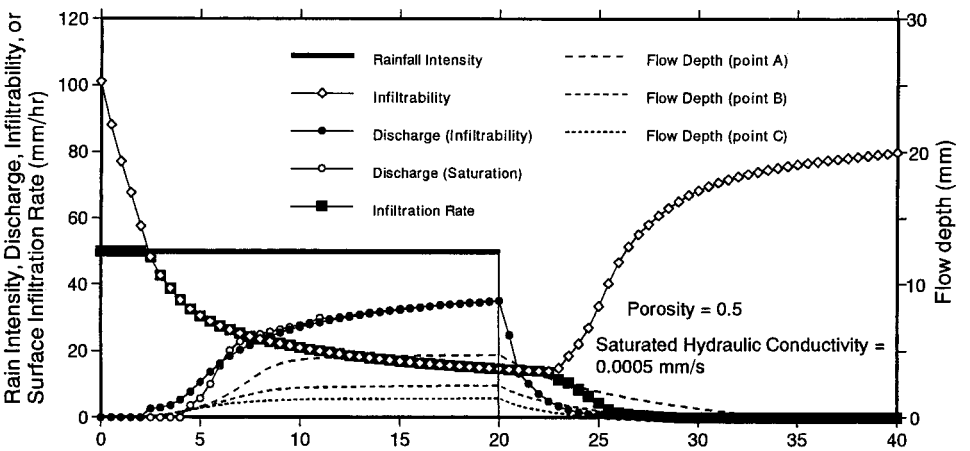

(b) Simulation Results from Rectangular Hyetograph

Fig. 10. Simulation results of conjunctive model for clay-type soil

Conjunctive Flow Model Simulation of Hortonian Overland Flow

As an example, the conjunctive model is applied to a hypothetical drainage plot (Fig. 8) to simulate the Hortonian runoff under a given rainfall to study the initial loss, onset of surface flow, overland flow, surface infiltration, and unsaturated subsurface flow. Freeze (1972b) defined the Hortonian runoff as *overland flow due to surface saturation from above*. Fig 8 shows a top view of the drainage plot. The surface flow area is 10 m by 10 m and has a slope 0.001 in both x and y directions. In the lower part of the figure is the cross sectional view showing the soil layers and the initial water table of the unconfined groundwater. For the surface flow the boundary condition consists of three closed sides and one open side connected to the channel shown as the right most boundary in the top view of Fig. 8. The conditions of example conjunctive model simulations are given in Table 2 as cases I–IV.

Two types of soil were tested, clay and sand, with their P-S and Kr-S curves shown in Fig. 9. The clay-type soil has hydraulic properties shown as curves A and 1, and those for the sand-type soil are given as curves B and 2 in the figure. The values of saturated hydraulic conductivity for the clay-type soil and the sand-type soil are 0.0005 and 0.005 mm/s, respectively.

Conditions of Numerical Calculation

For numerical calculation of the surface flow [Eq. (23)], the drainage plot has the space increments $\Delta x = \Delta y = 1.0$ m. For calculation of subsurface flow [Eqs. (24)–(26)], space increments are $\Delta x = \Delta y = 1.0$ m and $\Delta z = 0.01$ m. The time increment is $\Delta t = 1.0$ s. The soil moisture is assumed initially in a static equilibrium under piezometric head determined by the groundwater table. In other words, the initial capillary head changes linearly from zero at the groundwater table to -1.0 m near the soil surface. The upper soil boundary condition is represented by the procedure of the coupling of surface and subsurface flow components as previously described and shown in Fig. 1. The subsurface flow boundary conditions of the four sides are assumed to be impermeable as shown in Fig. 8.

Results of Conjunctive Flow Model Simulation

The hydrograph for the clay-type soil calculated for a triangular hyetograph with a peak rainfall intensity 100 mm/h (case I) is shown in Fig. 10(a). The figure describes rainfall intensity, surface flow discharges, surface infiltration rate, and infiltrability. Surface flow discharges were calculated by using two different

J. Hydraul. Eng. 2002.128:184-200.

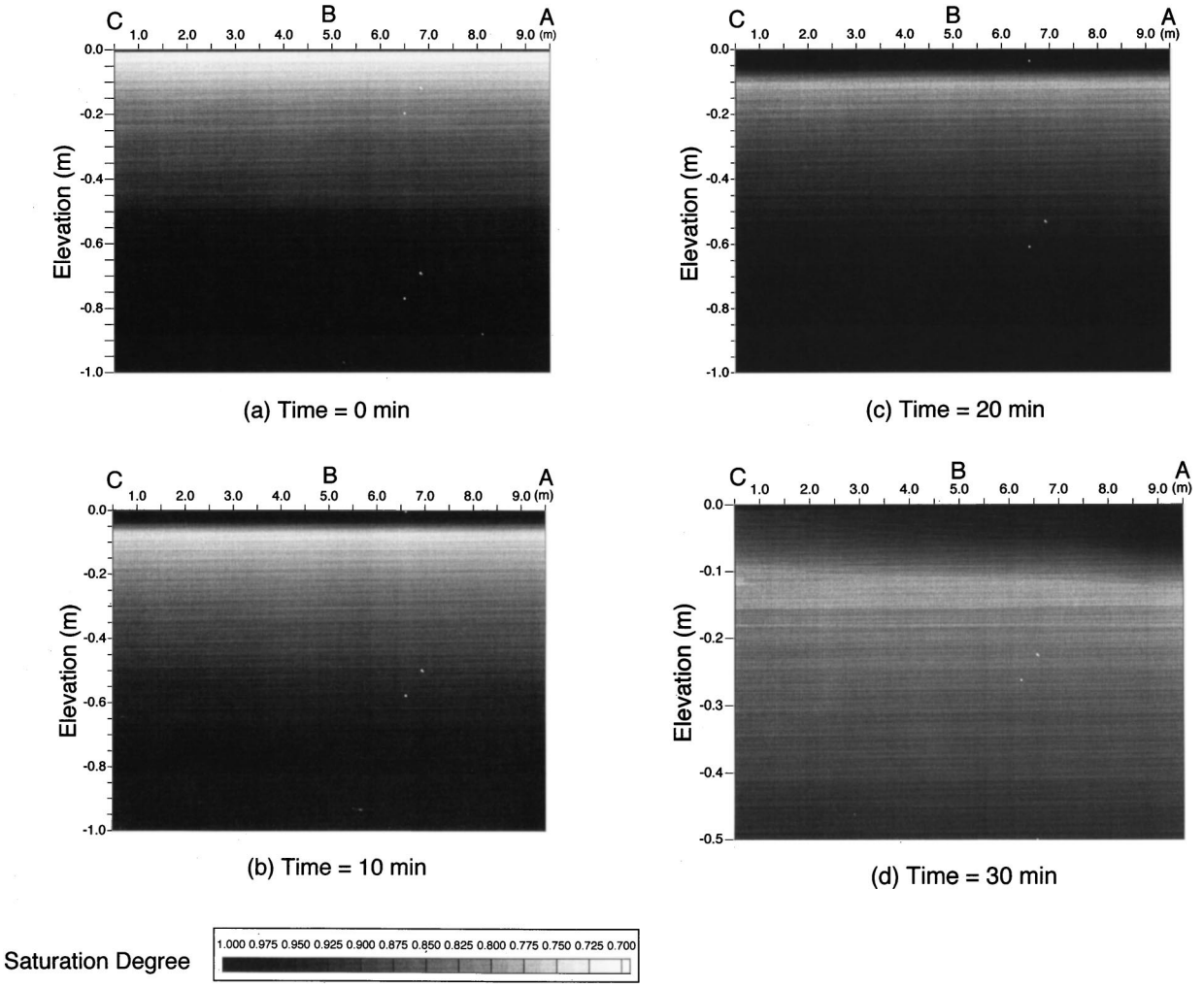

Fig. 11. Saturation degree profiles at cross section b-b in Fig. 8 for clay-type soil under rectangular hyetograph

methods to describe the common internal boundary for coupling, namely, the infiltrability method and the saturation method. In the figure the infiltration rate and the infiltrability shown are areal averaged values over the drainage plot. Each of the simulations shown in Fig. 10 required about 20 min using a personal computer (IBM PC with a clock frequency of 366 MHz).

The initial loss process occurs in the first 5 min when the infiltration is identical with the rainfall intensity. During the initial

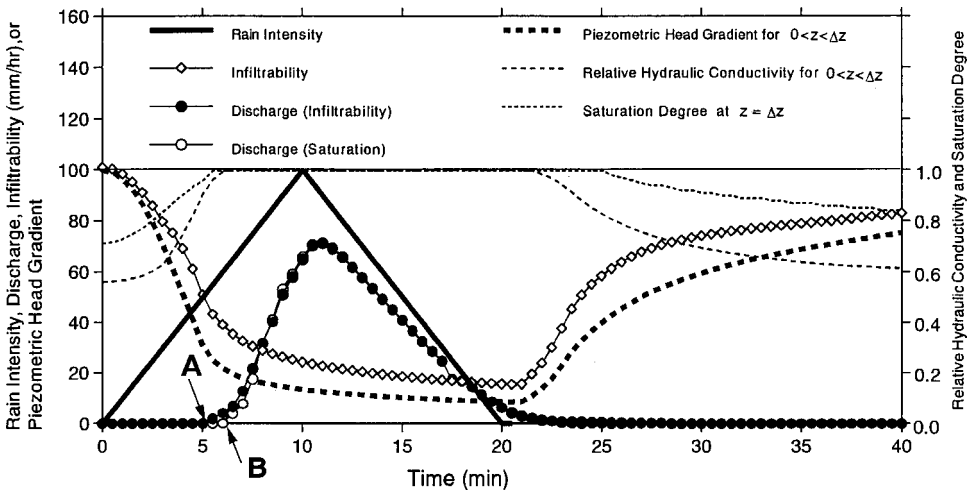

Fig. 12. Time variation of rain intensity, infiltrability, and discharge with piezometric head gradient, relative hydraulic conductivity for $0<z<\Delta z$, and saturation degree at $z=\Delta z$ in Fig. 10(a), clay-type soil.

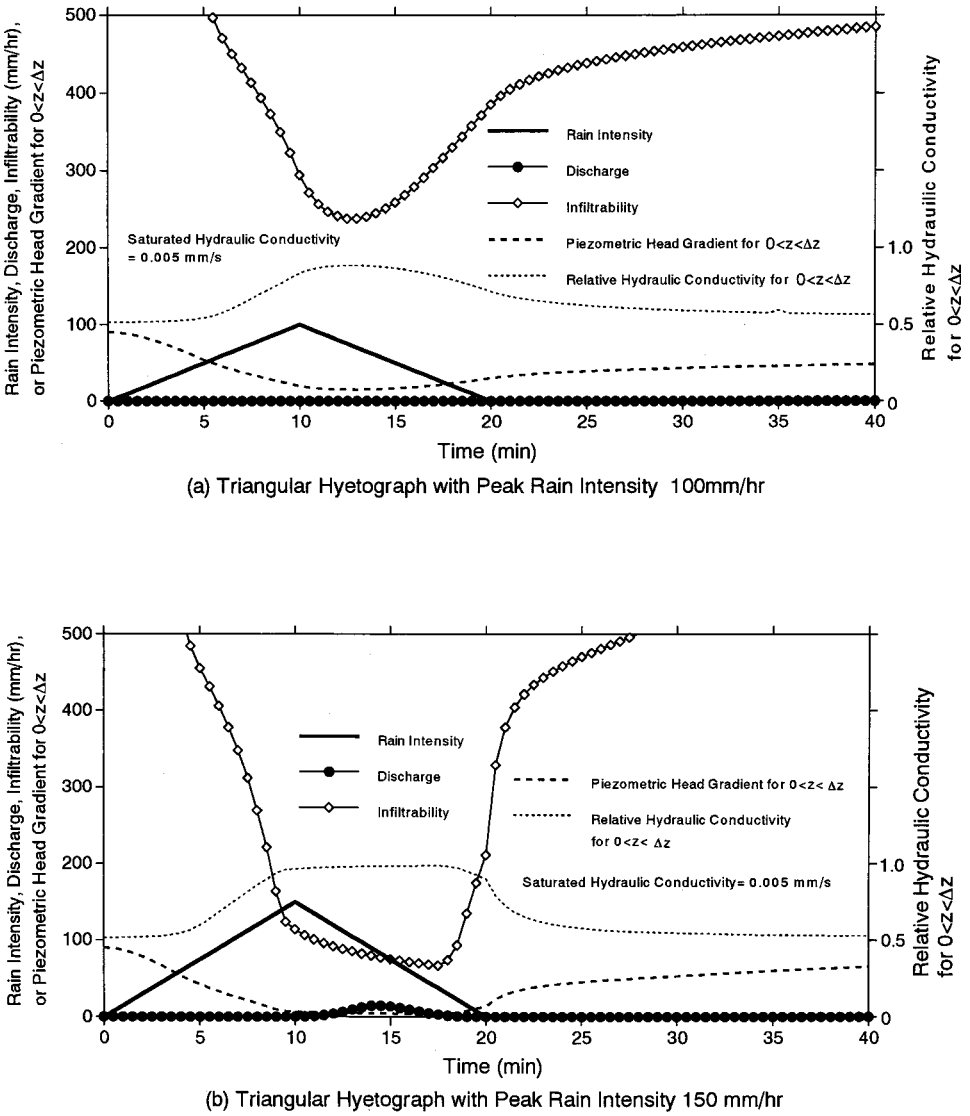

Fig. 13. Simulated results of conjunctive model for sand-type soil under triangular hyetograph

loss period, the infiltrability is larger than the rainfall intensity or rainwater supply. Overland flow follows after the initial loss period and reaches the peak discharge around 11 min, slightly after the peak rain intensity.

Fig. 10(a) also shows the surface flow depths at points A, B, and C in Fig. 8. The flow depth at point A is the largest and the depths at points B and C decrease in order. The three flow depth curves indicate that the times of initiation and termination of the overland flow differ at the three location points. In the calculation, part of the plot had overland flow while the rest of the plot had no water on the surface. The surface flow submodel thus simulates two-dimensional overland flow as expected. At the time of peak water depth, the discharge plus the infiltration rate should be equal to the rainfall intensity from the viewpoint of water balance. This relation can be found at 11.5 min in Fig. 10(a).

The infiltrability shown in Fig. 10(a) decreases with decreasing piezometric head gradient and increasing hydraulic conductivity of the very thin soil layer at the ground surface. The infiltrability curve has an inflection point at the early stage of rainfall. The overland flow calculated by the infiltrability method initiates when the infiltrability curve meets the hyetograph at about 5 min. After the rain has stopped and the surface water flow decreases, the recovery of infiltrability or infiltration capacity can be recognized. Thereafter the infiltrability again becomes larger than the rainwater supply and no water flows on the surface.

The overland flow calculated by the infiltrability method initiates earlier than that calculated by the saturation method in Fig. 10(a). This simulation result signifies overland flow which occurs when the rain intensity exceeds the infiltrability even if the surface layer of the soil is still unsaturated.

The hydrograph calculated for the clay-type soil under a rainfall of constant intensity, i.e., a rectangular hyetograph (case II), is presented in Fig. 10(b). The curves of discharge and infiltration are simpler than those in Fig. 10(a). The infiltrability curve decreases monotonically with no inflection point, in a manner similar to Horton's empirical infiltration formula curve. The overland flow initiates just as the infiltrability curve meets the hyetograph as in the case of Fig. 10(a). The overland flow calculated by the infiltrability method initiates earlier than that calculated by the saturation method [Fig. 10(b)], and earlier than those for the triangular hyetograph [Fig. 10(a)].

Fig. 11 shows the cross sectional view of variation of saturation degree over depth and time, thus describing the soil moisture movement, for case II. The saturation degree at cross section a-a

J. Hydraul. Eng. 2002.128:184-200.

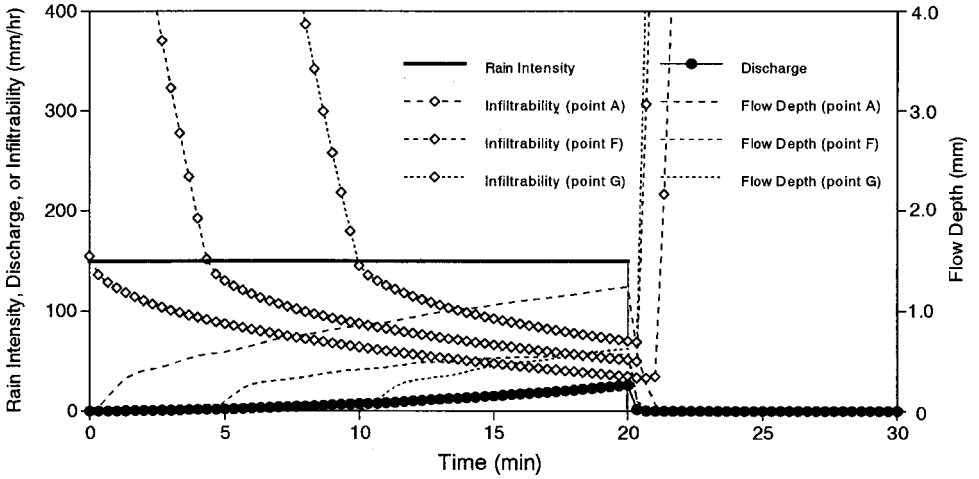

Fig. 14. Simulated hydrograph under rectangular hyetograph for clay-type soil saturation overland flow

in Fig. 8(a) is presented. At the beginning of the rainfall, there is no infiltration and capillary rises from the unconfined groundwater table are shown in Fig. 11(a). Once rainfall begins, soil moisture moves vertically down from the surface and the wetting front propagates uniformly as shown in Figs. 11 (b and c). After the rain ceases at 20 min, overland flow and depth decrease gradually. As shown in Fig. 10(b), overland flow terminates differently in time at points A, B, and C. It terminates at about 24 min at point C. For point A, the flow lasts until 32 min. This difference in overland flow duration causes horizontally nonuniform saturation degree distribution in the soil. In Fig. 11(d), the saturation degree in the soil around point A is larger than any other portion of the soil near the surface. Fig. 11 presents a typical soil moisture movement of Hortonian overland flow.

Discussions on Hortonian Overland Flow

In the conventional approach like Horton's formula, the same soil condition produces the same infiltrability, even if the hyetograph is different. The conjunctive model, however, gives different infiltrability as shown in Figs. 10(a and b). Overland flow and infiltration depend on the relationship between infiltrability and rainwater supply as described in the flow chart in Fig. 1. Over the duration of runoff processes the infiltrability and rainwater supply are not independent, but the former is influenced by the latter. The infiltrability is neither constant in time nor a function of only time elapsed, unlike that given by Horton's infiltration formula as used in uncoupled modeling.

In this paper, the infiltrability is defined by Eq. (18) which indicates that the infiltrability is determined by the unsaturated hydraulic conductivity K_1 and piezometric head H_1 at $z=\Delta z$, as well as the saturated hydraulic conductivity K_{sz} at $z=0$. The depth of water available Y from rainfall is the piezometric head at $z=0$. These factors, except the saturated hydraulic conductivity, change with time and are influenced by rainfall. For the first Δz, at the ground surface the saturated hydraulic conductivity K_s is used as the hydraulic conductivity in Eq. (18).

The soil hydraulic properties and the initial soil moisture condition are the same for the two simulations of Figs. 10(a and b). In Figs. 10(a and b), it can be seen that the infiltrability changes in time with rainfall. However, the infiltrability curves are not the same because the rainfalls are different. The infiltrability in Fig. 10(b) with larger rainfall intensity decreases more rapidly than that in Fig. 10(a), especially in the first 2 min. At the early stage of the triangular hyetograph increasing rain intensity causes an inflection point in the infiltrability curve in Fig. 10(a). The rainwater supply brings about decreasing piezometric head gradient and increasing unsaturated hydraulic conductivity near the ground surface. In Figs. 10(a and b), in the early period the decreasing piezometric head gradient overwhelmed the increasing unsaturated hydraulic conductivity, causing the infiltrability to decrease monotonically. When the rainfall ceased, the infiltrability recovered temporarily because of increasing piezometric head gradient.

To confirm the relations stated previously, Fig. 12 shows the variations in rain intensity, infiltrability, and discharge in Fig. 10(a) with the piezometric head gradient and the relative hydraulic conductivity at the surface, and the saturation degree just below the surface. As can be seen easily, the piezometric head

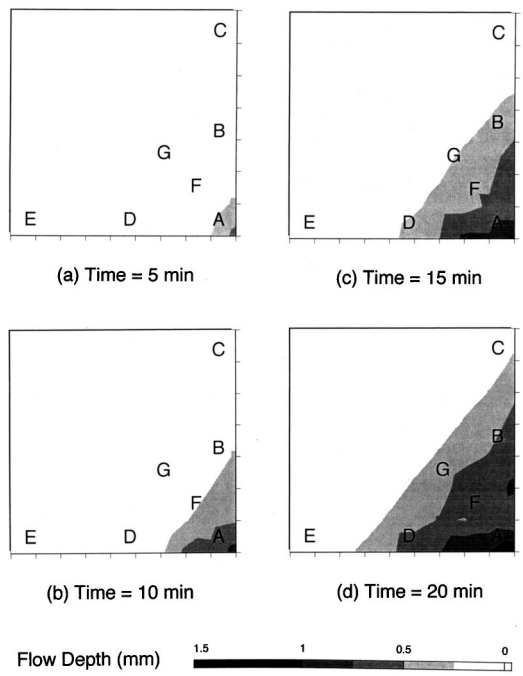

Fig. 15. Propagation of partial contribution area of saturation overland flow on clay-type soil plot of Fig. 8

J. Hydraul. Eng. 2002.128:184-200.

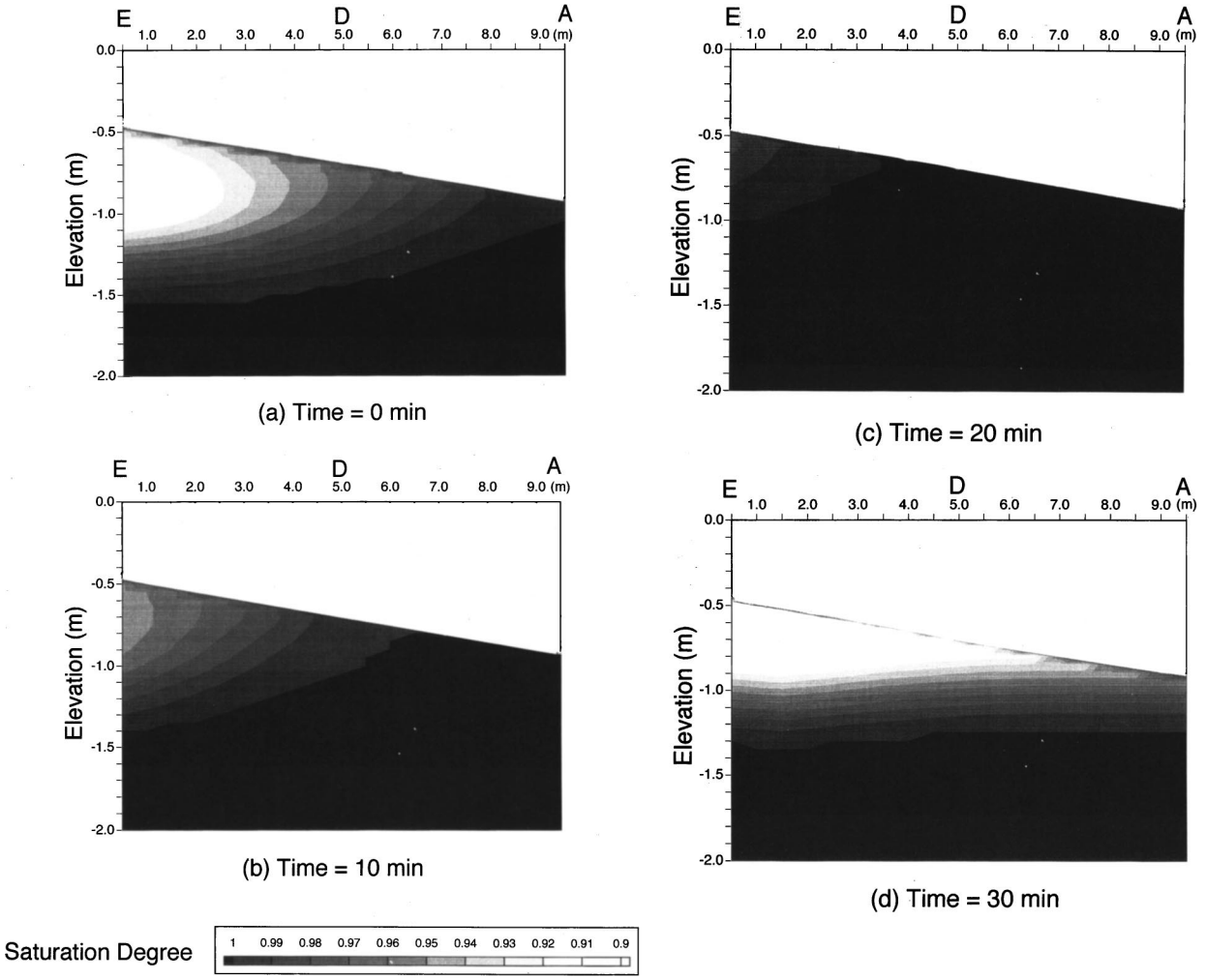

Fig. 16. Saturation degree profiles for saturation overland flow at cross section a-a in Fig. 8 for clay-type soil under rectangular hyetograph

gradient decreases more rapidly than the relative hydraulic conductivity increases, resulting in the decrease in infiltrability. Recovery of the infiltrability can be explained by the increase in the piezometric head gradient because of the decrease in soil moisture just below the surface shown in Fig. 12.

Fig. 12 depicts the discharges calculated by using the two different flow initiation methods. For the discharge from the infiltrability method, overland flow initiates at $t=5$ min (point A) when the rain intensity curve meets infiltrability curve. On the other hand, overland flow from the saturation method initiates at $t=6$ min (point B) when the saturation degree at $z=\Delta z$ becomes 1.0. Some conjunctive models using the saturation method adopt the criterion that overland flow occurs when rain intensity exceeds the infiltration capacity (infiltrability) of the saturated soil surface, based on the saturated hydraulic conductivity and piezometric head gradient equal to unity for Hortonian overland flow generation. However, as Fig. 12 shows, while the piezometric head gradient decreases with saturation of the soil surface, it remains greater than 1.0. This is because saturation of the soil surface does not necessarily mean the capillary pressure equals zero, as is shown in Fig. 5 and in Fig. 9.

In addition to the clay-type soil, conjunctive model calculations were carried out for the sand-type soil (B-2) shown in Fig. 9. Saturated hydraulic conductivity was set as $K_s=0.005$ mm/s for the fine sand. With a triangular hyetograph having a peak rain intensity of 100 mm/h (case III), the calculation yields no overland flow as depicted in Fig. 13(a), because the infiltrability of the pervious sand-type soil is much larger than the rain intensity. For a triangular shaped hyetograph with peak rain intensity of 150 mm/h (case IV) in Fig. 13(b), overland flow initiates when the rainfall intensity becomes larger than the infiltrability. In Figs. 13(a and b), piezometric head gradient and relative hydraulic conductivity at the surface are also given to explain the curves of infiltrability.

Example of Conjunctive Flow Model Simulation of Saturation Generated Overland Flow

A special case of Hortonian overland flow is saturation overland flow for which the soil is saturated at the beginning of rainfall from previous water supply or high groundwater level. This is especially common in the soil near the bottom of a slope. Freeze (1972b) refers to this type of overland flow as *overland flow from near-channel partial areas due to surface saturation from below*. The conjunctive model was applied to a simulation example of such 3D saturated subsurface flow and 2D overland flow.

The drainage plot shown in Fig. 8 is slightly modified for the saturation overland flow simulation. The drainage plot calculation conditions, except the slopes of the surface flow and the uncon-

J. Hydraul. Eng. 2002.128:184-200.

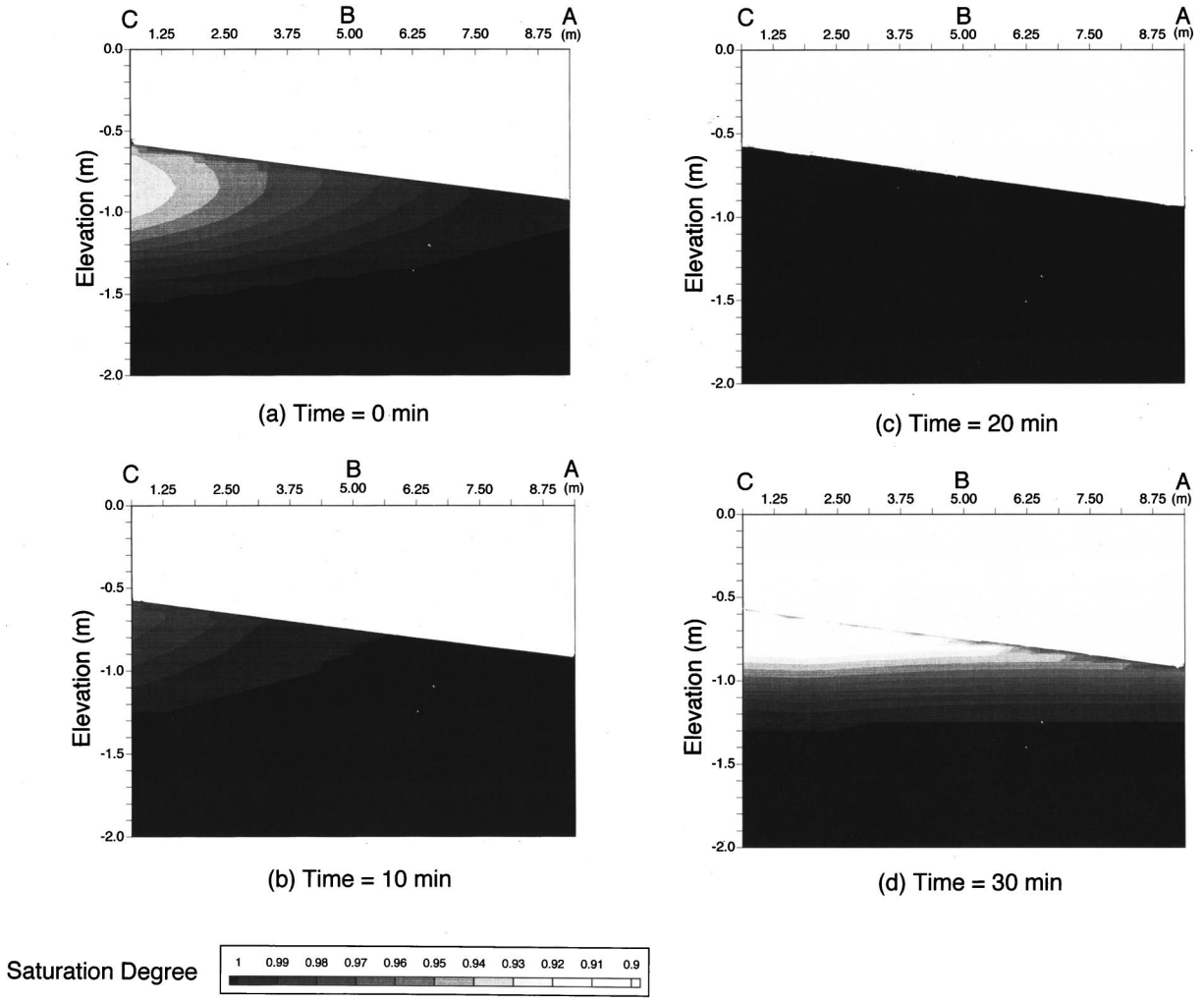

Fig. 17. Saturation degree profiles for saturation overland flow at cross section b-b in Fig. 8 for clay-type soil under rectangular hyetograph

fined groundwater table for the subsurface flow, are the same as in Fig. 8. The slopes of the surface flow area are 0.05 and 0.04 in the x and y directions, respectively. Point A is situated at the bottom of the simplified 2D hill slope where saturation overland flow first occurs. The soil used in the calculation has clay-type hydraulic property with saturated hydraulic conductivity 0.05 mm/s as permeable loam. The space increments for subsurface flow calculation are $\Delta x = \Delta y = 1.0$ m and $\Delta z = 0.05$ m and the time increment is $\Delta t = 0.1$ s. The initial condition was defined such that overland flow was just initiating at A. In order to ensure model stability, this was achieved by simulating a rainfall with a constant intensity of 150 mm/h for 14 min preceding the start of the simulation for the example conditions. The soil saturation degree distributions at the cross sections a-a and b-b in Fig. 8 at time $t = 0$ min are shown in Figs. 16(a) and 17(a), respectively. This simulation required about 30 min on the PC used.

Fig. 14 shows the simulated hydrograph from a 20 min rectangular hyetograph with a constant rainfall intensity of 150 mm/h. The infiltrabilities and surface flow depths at points A, F, and G of Fig. 8 are shown in Fig. 14. Relationships among rainfall, infiltrability, and discharge for saturation overland flow shown in Fig. 14 are basically the same as for Hortonian overland flow shown in Fig. 10(b). The infiltrability decreases with rainfall and the overland flow occurs when the infiltrability curve meets the rain intensity curve at 0, 5, and 11 min for point A, F, and G, respectively. Comparison between infiltrability and rain intensity is proved to be essential for the initiation of overland not only for Hortonian overland flow but also for saturation overland flow. Overland flow in the saturation case, however, is produced from a portion of the drainage surface while the overland flow initiates over the entire plot in the Hortonian case. Fig. 15 depicts the partial contribution area of overland flow propagating upstream from the bottom of the slope. Overland flow is initiated when rainwater supply exceeds infiltrability in both Hortonian and saturation overland flows.

Similar to the Hortonian overland flow case, soil moisture changes for cross sections a-a and b-b [Fig. 8(a)] are presented in Figs. 16 and 17, respectively. At time $t = 0$, the soil at point A is saturated over the entire depth as shown in Fig. 16(a). The soil moisture changes with time in these figures; however, the change is different from that of Hortonian overland flow shown in Fig. 11. For saturation overland flow soil surface saturation proceeds from the lower to the upper portions of the plot, whereas for Hortonian overland flow the soil surface is saturated directly by infiltration. As shown in Fig. 15, the partial contribution area propagates from point A toward points F, D, and B. This can be seen in Figs. 16(b and c) and in Figs. 17(b and c). The difference in the slopes in the x and y directions causes the difference in saturation degree change shown in Figs. 16 and 17. Overland flow on the smaller slope continues longer than that on the larger slope

and thus the saturated portion in Fig. 16 is smaller than that in Fig. 17. After the rain ceases at 20 min, the soil moisture begins to recede from saturated to unsaturated conditions, beginning at the upstream part of the plot and progressing downward. The soil moisture distribution after 30 min is shown in Figs. 16(d) and 17(d). The conjunctive model calculation thus shows the 3D soil moisture movement by the expansion and redistribution of the saturated portion, and correspondingly the 2D surface flow shown by propagation of the partial contribution area.

Conclusions

A PC-based simulation model for conjunctive two-dimensional surface and three-dimensional subsurface flows can be established for application to water resources problems such as farmland runoff, infiltration trenches, irrigation and drainage, porous-bed ponding, groundwater recharge through infiltration and porous pavement. In the current study, the 2D surface flow is represented by the noninertia approximation of the Saint-Venant equation and the 3D variably saturated flow is represented by the Richards equations. These equations are written in the form of the heat diffusion equation and solved numerically and iteratively between the surface and subsurface components using infiltration as the common internal boundary condition. At each time step the infiltration rate is determined by comparing the water supply with the infiltrability (infiltration capacity).

The model has been verified with the 1D surface and 1D subsurface flow experimental data of Smith and Woolhiser (1971) and further tested for various flow and soil conditions. The example simulated results clearly show the interaction between surface runoff, infiltration, subsurface flow, wetting front propagation, and soil properties, as well as their relation with the external water supply: rainfall. Thus, the model provides a basic tool to investigate and to explain the physics of various runoff phenomena.

Notation

The following symbols are used in this paper:

D_x, D_y = diffusion coefficients for surface flow;
f_d = overland flow resistance coefficient;
g = gravitational acceleration;
H_s = water surface elevation;
H = piezometric head;
H_0 = piezometric head at ground surface as boundary condition;
H_1 = piezometric head at first node in z direction;
h = overland flow depth;
Ip = infiltrability;
i = infiltration rate;
K_{sx}, K_{sy}, K_{sz} = saturated soil hydraulic conductivity in x, y, and z directions, respectively;
K_r = unsaturated relative hydraulic conductivity;
K_1 = soil hydraulic conductivity at the first node in the z direction;
k_s = equivalent sand grain roughness size;
n = soil porosity;
P = capillary pressure head;
R = Reynolds number;
R = hydraulic radius of surface flow;
R_s = rainwater supply;
r = rainfall intensity;
S = soil saturation degree;
S_{fx}, S_{fy} = friction slopes of overland flow in x and y directions;
S_{0x}, S_{0y} = overland surface slopes in x and y directions;
s = overland surface elevation;
t = time;
U, V = intermediate values of piezometric head H in numerical calculation;
u, v = surface flow depth average velocity components in x and y directions, respectively;
u_r = velocity of rainwater when joining surface flow;
V_m = mean velocity over depth of overland flow;
x, y, z = spatial coordinates;
Y = available water from rain and surface flow;
θ = volumetric soil moisture content; and
ν = kinematic viscosity of fluid.

References

Abbott, M. B., Andersen, J. K., Havnø, K., Jensen, K. H., Kroszynski, U. I., and Warren, I. R. (1982). "Research and development for the unsaturated zone component of the European Hydrologic System—Systeme Hydrologique European (SHE)," in *Engineering applications of computational hydraulics*, M. B. Abbott and J. A. Cunge, eds., Pitman, London, Vol. 1, 40–70.

Abbott, M. B., Bathurst, J. C., Cunge, J. A., O'Connell, P. E., and Rasmussen, J. (1986). "An introduction to European Hydrological System—Systeme Hydrologique European, SHE, 2: Structure of a physically-based distributed modeling system," *J. Hydrol.*, 87, 61–77.

Akan, A. O., and Yen, B. C. (1981a). "Mathematical model of shallow water flow over porous media," *J. Hydraul. Div., Am. Soc. Civ. Eng.*, 107(4), 479–494.

Akan, A. O., and Yen, B. C. (1981b). "Diffusion-wave flood routing in channel networks," *J. Hydraul. Div., Am. Soc. Civ. Eng.*, 107(6), 719–732.

Akanbi, A. A., and Katopodes, N. D. (1988). "Model for flood propagation on initially dry land," *J. Hydraul. Eng.*, 114(7), 689–706.

Bathurst, J. C., Wicks, J. M., and O' Connell, P. E. (1995). "Chapter 16: The SHE/SHESED basin scale water flow and sediment transport modelling system," in *Computer models of watershed hydrology*, V. P. Singh, ed., Water Resources, Highlands Ranch, Colo., 563–594.

Bradford, S. F., and Katopodes, N. D. (1998). "Nonhydrostatic model for surface irrigation," *J. Irrig. Drain Eng.*, 124(4), 200–212.

Di Giammarco, P., Giardino, P. T., Rametta, F., and Todini, E. (1994). "Integrated catchment modeling and meso-scale hydrology," in *Advances in distributed hydrology*, edited by R. Rosso, A. Peano, I. Becchi, and G. A. Bemporad, Water Resources, Highland Ranch, Colo., 247–292.

Freeze, R. A. (1972a). "Role of subsurface flow in generating surface runoff: 1. Base flow contribution to channel flow," *Water Resour. Res.*, 8(3), 609–623.

Freeze, R. A. (1972b). "Role of subsurface flow in generating surface runoff: 2. Upstream source areas," *Water Resour. Res.*, 8(5), 1272–1283.

Freeze, R. A., and Cherry, J. A. (1979). *Groundwater*, Prentice–Hall, Englewood Cliffs, N.J.

Hanks, R. J., and Bower, S. A. (1962). "Numerical solution of the moisture flow equation for infiltration into layered soils," *Soil Sci. Soc. Am. Proc.*, 26, 530–534.

J. Hydraul. Eng. 2002.128:184-200.

Horton, R. E. (1933). ''The role of infiltration in the hydrologic cycle,'' *Trans., Am. Geophys. Union*, 14, 446–460.
Horton, R. E. (1935). ''Surface runoff phenomena,'' Horton Hydrological Lab., Voorheesville, N.Y.
Izzard, C. F. (1946). ''Hydraulics of runoff from developed surfaces,'' *Proceedings Highway Research Board*, 26, 129–146.
Katopodes, N. D., and Strelkoff, T. (1977). ''Hydrodynamics of border irrigation: Complete model,'' *J. Irrig. Drain. Div. Am. Soc. Civ. Eng.*, 103(3), 309–324.
Larkin, B. K. (1964). ''Some stable explicit difference approximation to the diffusion equation,'' *Math. Comput.*, 18, 196–202.
Liggett, J. A., and Dillon, P. J. (1985). ''A dynamic model of flow exchange between streams and aquifers,'' *Proc. IAHR 21st Congress*, Melbourne, Australia, 1, 17–22.
Morita, M., and Yen, B. C. (2000). ''Numerical methods for conjunctive 2-D surface-3-D subsurface flow model,'' *Int. J. Numer. Methods Fluids*, 32 (8) 921–957.
Philip, J. R. (1957). ''The theory of infiltration: 1. The infiltration equation and its solution,'' *Soil Sci.*, 83(5), 345–357.
Philip, J. R. (1969). ''Theory of infiltration,'' *Advances in hydroscience*, V. T. Chow, ed., Academic, New York, Vol. 5, pp. 215–296.
Pinder, G. F., and Sauer, S. P. (1971). ''Numerical simulation of flow wave modification due to back storage effects,'' *Water Resour. Res.*, 7(1), 63–70.
Playan, E., Walker, W. R., and Merkley, G. P. (1994). ''Two-dimensional simulation of basin irrigation, 1: Theory,'' *J. Irrig. Drain Eng.*, 120(5), 837–856.
Reeder, J. W., Freyberg, D. L., Franzini, J. B., and Remson, I. (1980). ''Infiltration under rapidly varying surface water depths,'' *Water Resour. Res.*, 16(1), 97–104.
Refsgaard, J. C., and Storm, B. (1995). ''Chapter 23: MIKE SHE,'' in Ref. 6, 809–846.
Rubin, J., and Steinhardt, R. (1963). ''Soil water relation during rain infiltration: 1. Theory,'' *Soil Sci. Soc. Proc.*, 246–251.
Saul' yev, V. K. (1964). *Integration of equations of parabolic type by the method of nets*, Macmillan, New York.
Savadi, M. R. (1993). ''Modeling subsurface drainage and surface runoff with WEPP,'' *J. Irrig. Drain Eng.*, 119(5), 801–813.
Schmitz, G., Haverkamp, R., and Palacios, V. O. (1985). ''A coupled surface-subsurface model for shallow water flow over initially dry soil,'' in Ref. 18, 23–30.
Singh, V., and Bhallamudi, S. M. (1996). ''Complete hydrodynamic border-strip irrigation model,'' *J. Irrig. Drain Eng.*, 122(4), 189–197.
Smith, R. E., and Woolhiser, D. A. (1971). ''Overland flow on an infiltration surface,'' *Water Resour. Res.*, 7(4), 899–913.
Swartzendruber, D., and Hillel, D. (1973). ''The physics of infiltration,'' in *Physics of soil, water and soil in ecosystems*, A. Hadas et al., eds., Springer, Berlin.
Wallach, R., Grigorin, G., and Rivlin, J. (1997). ''The errors in surface runoff prediction by neglecting the relationship between infiltration rate and overland flow depth,'' *J. Hydrol.*, 200, 243–259.
Yen, B. C. (1973). ''Open-channel flow equations revisited,'' *J. Eng. Mech. Div. Am. Soc. Civ. Eng.*, 99(5), 979–1009.
Yen, B. C. (1991). ''Hydraulic resistance in open channel,'' in *Channel flow resistance: Centennial of Manning's formula*, B. C. Yen, ed., Water Resources, Highlands Ranch, Colo., 1–135.
Yen, B. C., and Akan, A. O. (1984). ''Effect of soil property on overland flow and infiltration,'' *Proc. Third IAHR/IAWPRC Conference on Urban Storm Drainage*, Goteborg, Sweden, 193–202.
Yen, B. C., and Akan, A. O. (1999). ''Chapter 14: Hydraulic design of urban drainage systems,'' *Hydraulic design handbook*, L. W. Mays, ed., McGraw–Hill, New York, pp. 14.1–14.114.
Yen, B. C., and Riggins, R. (1991). ''Time scales for surface subsurface flow modeling,'' *Irrigation and Drainage, (Proc. ASCE National Conf.*, Honolulu), 351–358, ASCE, Reston, Va.
Yen, B. C., and Tsai, C. W.-S. (2001). ''On noninertia wave vs. diffusion wave in flood routing,'' *J. Hydrol.* (to be published).

J. Hydraul. Eng. 2002.128:184-200.